Nature of the ferromagnetic ground state in the Mn_4 molecular magnet

S. V. Streltsov,[1,*] Z. V. Pchelkina,[1,2] D. I. Khomskii,[3] N. A. Skorikov,[1] A. O. Anokhin,[1] Yu. N. Shvachko,[1] M. A. Korotin,[1] V. I. Anisimov,[1,2] and V. V. Ustinov[1]

[1]*Institute of Metal Physics, S. Kovalevskoy St. 18, 620990 Ekaterinburg, Russia*

[2]*Ural Federal University, Mira St. 19, 620002 Ekaterinburg, Russia*

[3]*II. Physikalisches Institut, Universität zu Köln, Zülpicher Straße 77, D-50937 Köln, Germany*

(Received 9 September 2013; revised manuscript received 15 January 2014; published 30 January 2014)

Using *ab initio* band-structure and model calculations, we studied magnetic properties of one of the Mn_4 molecular magnets $[Mn_4(hmp)_6]$, where two types of the Mn ions exist: Mn^{3+} and Mn^{2+}. The direct calculation of the exchange constants in the GGA + U approximation shows that in contrast to a common belief, the strongest exchange coupling is not between two Mn^{3+} ions (J_{bb}), but along two out of four exchange paths connecting Mn^{3+} and Mn^{2+} ions (J_{wb}). Within the perturbation theory, we performed the microscopic analysis of different contributions to the exchange constants, which allows us to establish the mechanism for the largest ferromagnetic exchange. In the presence of the charge order, the lowest in energy virtual excitations, contributing to the superexchange, will not be those across the Hubbard gap $\sim U$, but will be those between the Mn^{3+} and Mn^{4+} ions, which cost much smaller energy V ($\ll U$). Together with strong Hund's rule coupling and specific orbital order, this leads to large ferromagnetic exchange interaction for two out of four Mn^{2+}-Mn^{3+} pairs.

DOI: 10.1103/PhysRevB.89.014427 PACS number(s): 75.50.Xx, 75.25.Dk, 71.70.Ej

I. INTRODUCTION

The magnetic materials are so ubiquitous and essential for plenty of devices used in the everyday life that their properties are just taken for granted. The refrigerator magnets, medical implants, loudspeakers, magnetic resonance imaging scanners, magneto-optical disks, electrical motors, and generators, etc.: all these devices use permanent or nonpermanent magnets. Yet, such an ancient and customary phenomenon as magnetism offers plenty of amazing new aspects. One of them is the molecule-based magnetism discovered about two decades ago [1].

It was revealed that single-molecule magnets (SMMs) and single-chain magnets having large spin and strong easy-axis anisotropy can self-assemble into two- and three-dimensional (2D and 3D) networks. This gives a great hope that one bit of information could be stored on a single molecule [2]. The new multidisciplinary field developed at the interface of chemistry and solid-state physics was triggered by the finding that SMMs exhibit both classical and exotic quantum magnetic properties [3]. Challenged by the promising molecular spintronics and quantum computing applications, sophisticated SMMs based not only on 3*d* transition metals but also on the 4*d* and even on the lanthanide and actinide elements were developed [4–7]. The theoretical studies have mostly concentrated on the description of the resonant tunneling experiments [8,9], *ab initio* simulations [10–12], and investigation of the role of the correlation effects [13].

The single-molecule magnets consist of a core and bridging polynuclear complexes. The physical insight into the magnetic interactions within the core is essential for both fundamental and technological development. At present, the values of the exchange constants in SMMs are typically estimated by the fitting of the experimental magnetic susceptibility to some solution of the Heisenberg model. There are a number of deficiencies in such a strategy mainly related with the large number of fitting parameters and sometimes with an arbitrariness in the choice of the model Hamiltonian, which in general must include not only different direct and superexchange interactions, but also magnetocrystalline anisotropy, Dzyaloshinskii-Moriya terms, etc.

In this paper, we calculate the exchange constants in one of the Mn_4 molecular magnets $\{[Mn_4(hmp)_6(NO_3)_2FeNO(CN)_5]\cdot 4CH_3CN\}$ with two types of Mn ions (Mn^{2+} and Mn^{3+}) having "butterfly" geometry. Experimentally, it is established that the ground state of this molecule is ferromagnetic. It is commonly assumed that there are two exchange interactions in the Mn_4 molecule magnets: J_{bb} (body-body) between two Mn^{3+} ions and J_{wb} (wing-body) between Mn^{2+} and Mn^{3+} ions (see Fig. 1, where J_1 and J_2 are two different J_{wb}), both of which are ferromagnetic with the first being much larger than the second [14]. The direct calculations presented in this paper reveal that this accepted picture is in fact incorrect: the dominant ferromagnetic exchange is not J_{bb}, but J_{wb}, with two inequivalent J_{wb} being very different. The magnetic susceptibility obtained by the exact diagonalization method with the use of the calculated exchange integrals agrees with experimental data.

The detailed microscopic analysis shows that there are many exchange processes in the $Mn_4(hmp)_6$ molecular magnet, which partially compensate each other, but its magnetic properties are mainly defined by two features of this system. First of all, the Jahn-Teller distortions lead to a specific orbital order, which in turn makes two exchange paths between Mn^{2+} and Mn^{3+} ions inequivalent. Second, the charge order strongly modifies the exchange processes between Mn ions of different valences and favors ferromagnetic exchange coupling. The results obtained allow us not only to describe magnetic properties of the $Mn_4(hmp)_6$ molecular magnet, but can be applied to other systems, including transition-metal oxides, with a charge-ordered ground state. In conclusion, we suggest some recipes to increase the value of the ferromagnetic exchange in the Mn_4 molecule magnets on the basis of the

*streltsov@imp.uran.ru

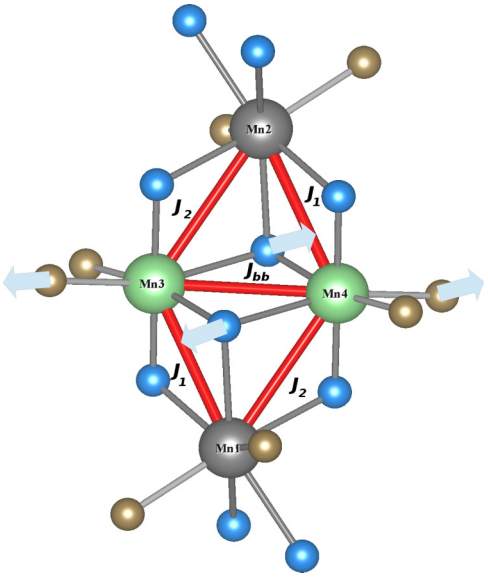

FIG. 1. (Color online) A fragment of the Mn_4 crystal structure is shown. The Mn^{2+} ions (Mn1 and Mn2) are shown as gray, Mn^{3+} (Mn3 and Mn4) as green, O as blue, and N as brown balls. Arrows show the direction of the Jahn-Teller elongation of the $Mn^{3+}O_6$ octahedra. The path for the "body-body" exchange coupling is labeled as J_{bb}, while two different "wing-body" exchange integrals are denoted via J_1 and J_2.

microscopic model developed in this study. We believe that the strategy presented here will be useful for other SMMs.

II. CRYSTAL STRUCTURE AND CALCULATION DETAILS

The crystal structure for system $[Mn_4(hmp)_6(NO_3)_2(H_2O)_2](ClO_4)_2{\cdot}4H_2O$, abbreviated as $Mn_4(hmp)_6$ in what follows, was taken from Ref. [15]. The main building block of $Mn_4(hmp)_6$ is the core consisting of four Mn ions (two Mn^{2+} and two Mn^{3+}) and surrounding ligands shown in Fig. 1. Since Mn^{3+} are Jahn-Teller active ions, the ligand octahedra surrounding them are strongly distorted. It was shown in Ref. [16] that in the case of identical ligands, the elastic interaction favors a parallel order of the elongated Mn-O bonds in the Jahn-Teller octahedra having a common edge. Surprisingly, this is also the case in $Mn_4(hmp)_6$.

Note right away that for the J_2 bonds (Mn1-Mn4 and Mn2-Mn3), the long Mn^{3+}-O bonds, shown in Fig. 1 by broad arrows, lie in the plane of corresponding Mn1-O-Mn4-O and Mn2-O-Mn3-O plaquettes, whereas for the bonds J_1 (Mn1-Mn3 and Mn2-Mn4), these long bonds are perpendicular to such plaquettes. As we show in the following, this will finally give very different exchange constants J_1 and J_2.

The band-structure calculations were performed within the density functional theory (DFT). This type of calculation was proven to provide adequate description of many organic compounds including mixed-valence systems [11,17,18], while some restrictions related with the computation of the low-spin states have to be mentioned [19]. The projector augmented wave (PAW) method as implemented in the Vienna *ab initio* simulation package (VASP) was used [20]. The exchange-correlation potential was chosen to be in Perdew-Burke-Ernzerhof (PBE) form [21]. Nonspherical contributions from the gradient corrections inside the PAW spheres were included in the calculation scheme. In order to take into account strong electronic correlations on the Mn sites, the GGA + U approximation (the generalized gradient approximation taking into account onsite U Hubbard correction) was applied [22] with the onsite Coulomb repulsion parameter $U = 4.5$ eV and the intra-atomic Hund's rule exchange $J_H = 0.9$ eV [23]. The spin-orbit coupling was not taken into account in the present calculations, so that the effects related to this interaction (such as, e.g., the single-ion anisotropy) were not considered.

The mesh of 8 **k** points was used in the course of the self-consistency. The integration of the bands was performed by the tetrahedron method with the Blöchl corrections [24]. The magnetic susceptibility was calculated using the exact diagonalization technique of the Heisenberg model

$$\hat{H} = 2J_{bb}\hat{S}_3\hat{S}_4 + 2J_1(\hat{S}_1\hat{S}_3 + \hat{S}_2\hat{S}_4) + 2J_2(\hat{S}_1\hat{S}_4 + \hat{S}_2\hat{S}_3) \quad (1)$$

implemented in the ALPS package [25]. The exchange constants J_{bb}, J_1, and J_2 were calculated from the total energies of four different magnetic configurations as discussed in Sec. III. The numeration of the spins and Mn ions in Eq. (1) and Fig. 1 is the same.

III. RESULTS OF THE CALCULATIONS AND COMPARISON WITH EXPERIMENT

The total and partial density of states (DOS) obtained in the GGA + U calculation for the fully ferromagnetic order [Fig. 2(a)] are presented in Fig. 3. One may see that the top

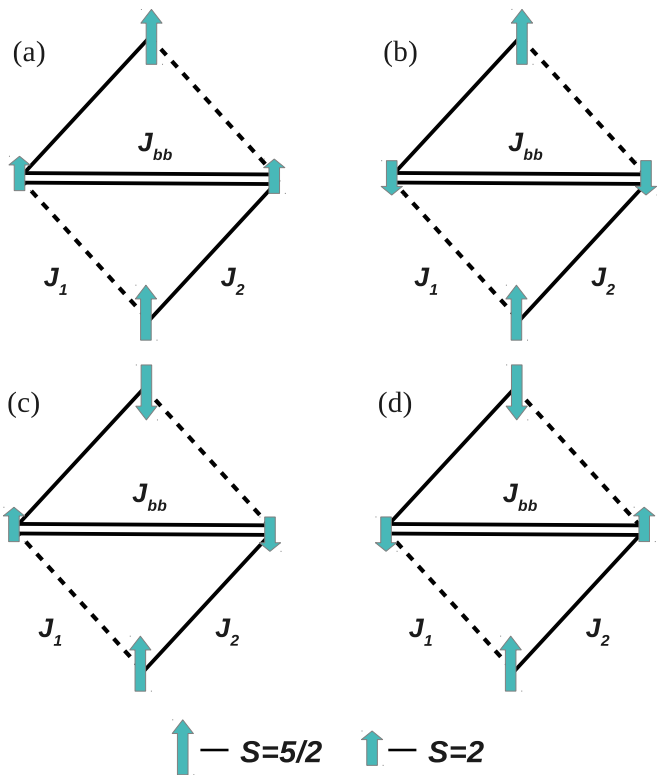

FIG. 2. (Color online) Magnetic configurations used for the exchange-coupling calculations.

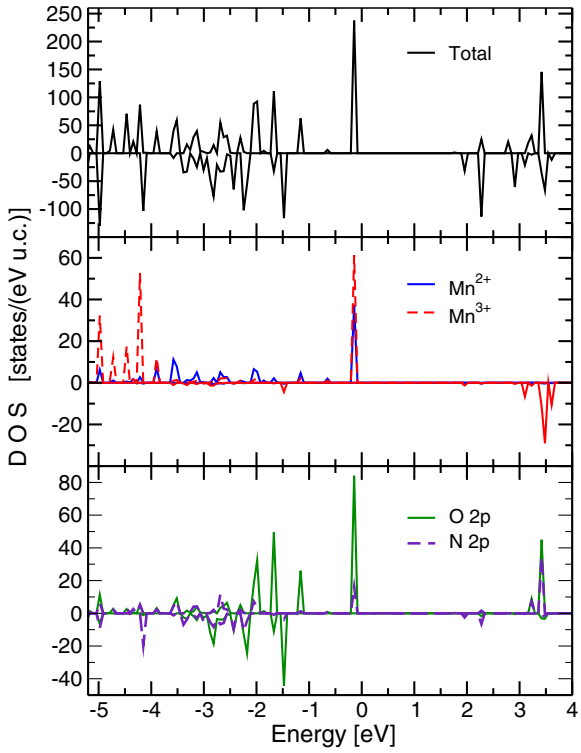

FIG. 3. (Color online) The total and partial density of states (DOS) of the Mn_4 obtained in the ferromagnetic GGA + U calculation. The positive (negative) values correspond to the spin-up (-down) states. The Fermi energy is in zero.

of the valence band is formed mostly by the O $2p$ states with admixture of the N $2p$, Mn^{3+} and Mn^{2+} $3d$ states. The lower Hubbard bands corresponding to the $3d$ states of the Mn^{3+} and Mn^{2+} ions are in the range from -5 to ~ -2 eV. The magnetic moments on the Mn^{2+} and Mn^{3+} were found to be $4.6\mu_B$ and $3.7\mu_B$, respectively. The deviations from the ionic values ($5\mu_B$ and $4\mu_B$) are related with the hybridization and covalency effects, which result in a transfer of a part of the spin density to the ligands. Similar effects were found in many other systems based on the transition-metal ions [26,27]. The lowest total energy corresponds to the magnetic configuration, when all Mn ions are ordered ferromagnetically.

As was already mentioned, typically only two exchange constants J_{bb} and J_{wb} are considered in the analysis of the magnetic properties of the Mn_4 molecular magnets [15,28]. In $Mn_4(hmp)_6$, J_{wb} is the exchange constant between Mn^{2+} and Mn^{3+}, and J_{bb} between two Mn^{3+}. However, a close inspection of the available crystal structure [15] shows that there are two different distances between the Mn^{2+} and Mn^{3+} ions: $d_1(Mn^{2+} - Mn^{3+}) = 3.28$ Å, and $d_2(Mn^{2+} - Mn^{3+}) = 3.34$ Å, which may result in two different exchange couplings J_{wb}. In order to check this hypothesis, we calculated total energies of four magnetic structures presented in Fig. 2, which allows us to extract three different exchange constants: $J_{bb}^{\rm Calc} = -0.3$ K, $J_1^{\rm Calc} = -6.3$ K, and $J_2^{\rm Calc} = -0.5$ K, all of which are ferromagnetic. Here, J_1 and J_2 are two inequivalent J_{wb} exchange couplings, which are shown in Figs. 1 and 2. This result is quite in contrast to the common opinion that J_{bb} must be much larger than any of J_{wb}.

The conventional assumption ($|J_{bb}| > |J_{wb}|$) was justified by two arguments. First of all, the Mn-Mn distance along the diagonal (3.20 Å in the present system) is much smaller than along the edges of the Mn_4 rhombus. Since the exchange constant in the simplest case [29]

$$J \sim \frac{t_{dd}^2}{U} \tag{2}$$

and the hopping integral for the d orbitals (t_{dd}) is supposed to be inversely proportional to the distance between ions $t_{dd} \sim 1/r^5$ [30], this viewpoint seems to be justified. However, the expression for the superexchange interaction in a particular situation can be quite different from Eq. (2). The detailed analysis performed in Sec. IV shows that for the given system, J_1 is indeed expected to be ferromagnetic and its absolute value is much larger than $|J_2|$ and possibly larger than $|J_{bb}|$.

Second, the values of the exchange constants are typically extracted from the fitting of the experimental magnetic susceptibility $\chi(T)$ by the theoretical curve obtained from the solution of the Heisenberg model [15,31]. There are three (g, J_{bb}, and J_{wb}) or even four (g, J_{bb}, J_1, J_2) fitting parameters, which results in an arbitrariness of this procedure. Instead of the fitting we first performed a direct calculation of the temperature dependence of χT (as described in Sec. II) with the exchange constants obtained in the band-structure calculations. The single variable parameter (g factor) was chosen to fit the high-temperature tail of χT and it was found to be equal to 1.86.

One may see from Fig. 4 that there is a reasonable agreement between calculated and experimental curves for $B = 0.01$ T. One may improve this agreement in the range from 20 to 100 K performing the fit to experimental data using calculated in the GGA + U exchange constants as a starting point. This yields $J_{bb}^{\rm fit} = -0.01$ K, $J_1^{\rm fit} = -6.5$ K, $J_2^{\rm fit} = -0.2$ K, and $g = 1.87$ K. Further improvement can be achieved by adding the single-ion anisotropy (via DS_z^2 terms for the Jahn-Teller

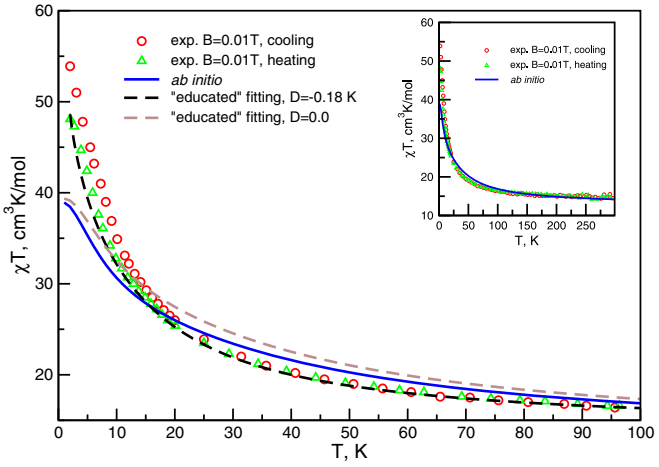

FIG. 4. (Color online) Temperature dependence of the experimental and calculated χT. All theoretical curves were obtained by exact diagonalization of the isotropic exchange interaction described by Hamiltonian (1) with the exchange constants, obtained in the GGA + U approximation, or using fitting taking into account or neglecting the single-ion anisotropy (D). χ is the molar susceptibility.

Mn^{3+} ions) into the fitting scheme. This gives $J_{bb}^{\text{fit},D} = -0.3$ K, $J_1^{\text{fit},D} = -3.6$ K, $J_2^{\text{fit},D} = -0.4$ K, $D^{\text{fit},D} = -0.18$ K, and $g = 1.94$ K. Thus, while J obtained in this "educated" fitting differs from those calculated in the GGA + U, the main result is the same: J_1 is the largest exchange constant. The difference between theoretical and experimental data for $T < 10$ K is related with experimental features of the measurements and $Mn_4(hmp)_6$ samples, as discussed in Sec. III A.

A. Low-temperature behavior of $\chi(T)T$: Experimental difficulties

Figure 5 discloses the details of measurements for the dried (aged) polycrystalline sample $[Mn_4(hmp)_6(NO_3)_2FeNO(CN)_5]4CH_3CN$ in Ref. [15]. Due to low-spin state $S = 0$, the Fe^{2+} ion does not contribute to the total paramagnetic response. Temperature dependencies for the product χT are obtained at magnetic fields $B = 0.01$ and 0.20 T. The measurements are performed at cooling from 300 down to 2.0 K and at heating to ambient conditions. The temperature axis in Fig. 5 is in logarithmic scale for better view of low-temperature behavior. While treatment of the mass of solvent acetonitrile molecules was subtracted from the total molecular weight, so that it was taken as 1208.448 g/mol. Solvent losses are a characteristic feature of $Mn_4(hmp)_6$ structures. Fresh crystals lose solvent with time, making the molar weight out of control, so that the error may reach 12%. Therefore, in this paper, the data for dry (aged) crystals left in the open dry air for several months were used.

One may see in Fig. 5 that the position of the low-temperature maximum of χT depends on the applied magnetic field B: it shifts to higher temperatures with increase of B. Such a behavior is common for most of the high-spin molecules and molecular magnets [3]. The origin of the maximum and its position in particular is not related with the microscopic characteristics of the exchange-coupled core. There are a few possible explanations of the low-temperature behavior of the experimental χT curve.

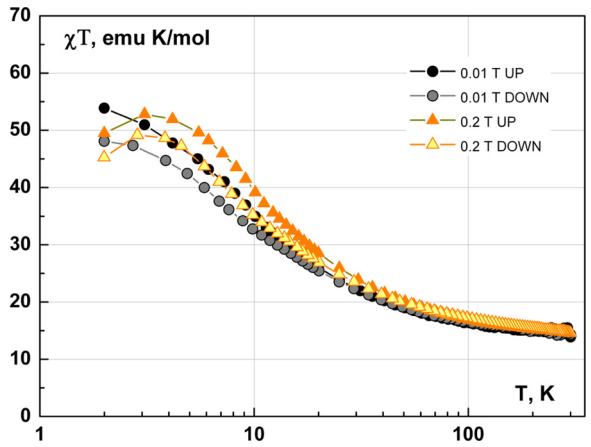

FIG. 5. (Color online) The experimental χT vs T data obtained for the polycrystalline sample in different magnetic fields $B = 0.01$ and 0.20 T for the cooling (DOWN) and heating (UP) regimes. The solid lines are guided by the eye.

First of all, in paramagnetic systems, the Curie law is only observed at temperatures $k_BT \gg g\mu_BSH$. For $T \lesssim T_p = g\mu_BSH$, thermal excitations are ineffective in providing dynamic Boltzmann equilibrium on higher Zeeman levels and the lowest level becomes "overpopulated." In theory, it means that one can not expand the Brillouin function in the Taylor series at $x \ll 1$ (where $x = g\mu_BSH/k_BT$) and get the Curie law. In practice, the data points will not lay on the equilibrium $\chi(T)T$ curve. For $B = 0.2$ T, where the maximum in $\chi(T)T$ is first clearly observable, $T_p = 2.4$ K and hence for the temperatures of order of T_p or lower the deviations from the Curie law have to be observed. This is exactly what is seen in Fig. 5. It is worthwhile mentioning that the stronger magnetic fields shift this region of the "inapplicability" of the Curie law to higher temperatures [32].

Second, there is no phase transition from correlated state (with spins $S_{Mn^{3+}} = 2$ and $S_{Mn^{2+}} = \frac{5}{2}$) to high-spin state $S = 9$ for the individual $Mn_4(hmp)_6$ complex as well as for other heterospin SMMs. Experimentally, there is no Curie temperature that can be measured. There is a temperature domain in which a crossover from a correlated paramagnetic to a high-spin superparamagnetic state occurs in an individual tiny single crystal. In this domain, both our Heisenberg model and dynamic $S = 9$ approach are not applicable. However, there is a blocking temperature $T_b \sim 1$–2 K, below which every complex in a tiny crystal becomes an anisotropic quantum magnet. In the measurement starting from that low temperature T_b, the magnetic response becomes quantitatively irreversible and dependent on magnetic history due to magnetic anisotropy of individual complex. In particular, this leads to a divergence of field-cooled (FC) and zero-field-cooled (ZFC) χT curves, as it happens in spin glasses. The FC-type curves prevail in published data. A typical sample mass of order of 10 mg requires fields 1000 G and higher to get satisfactory paramagnetic response at 300 K. For more than 40 various $Mn_4(hmp)_6$ systems listed in Refs. [14,28,33], the experimental $\chi(T)T$ data were obtained at $B > 0.1$ T, so that a sharp peak was present on every curve. In the experimental protocols, $\chi(T)$ measurements are performed at heating from helium to ambient temperatures. They usually follow after magnetization field measurements $M(B)$, where the excursions to high fields $B = 5$ to 7 T take place. The dependence of that type inherits magnetic history of the sample and imports excessive (or deficient) magnetization from the low- to higher-temperature region. This makes a broader temperature domain inappropriate for numerical analysis.

Third, the magnetic fields as low as ~0.1 T are capable to produce a texture in thin polycrystalline magnets. For textured samples, the product $\chi(T)T$ reaches maximum at higher temperatures. Ignoring the anisotropy, the maximal $\chi(T)T$ values in the high-spin state are limited by 45 to 50 emu K/mol for $g = 2.0$ to 2.1, respectively. Note also that the g factor for the $S = 9$ state differs from its average value at high temperatures. As an example, a broad maximum of 42 emu K/mol at $T \approx 10$ K was observed in polycrystals of $[Mn_2Mn_2(teaH)_2(teaH_2)_2(O_2CPh)_4]\cdot 0.7MeCN\cdot 0.3EtOH$ nearly isostructural to the similar system not revealing it [34]. That might be an indication of a texture rather than drastic enhancement of exchange coupling.

For analysis, we select $\chi(T)T$ data points measured at $B = 0.01$ T in order to avoid the the effect of the "overpopulation" of the lowest Zeeman level and reduce T_p as described above. Two sets of data "at cooling" and "at heating," presented in Fig. 4, allow us to estimate the difference between these regimes. Down to 20 K, both data coincide with the accuracy of 3.5%. At 2.0 K, the data diverge reaching 48.1 emu K/mol "at cooling" and 53.9 emu K/mol "at heating." The values 14.3 emu K/mol at 300 K are in agreement with other results reported on $Mn_4(hmp)_6$ structures and with the theoretical value 13.90 emu K/mol for $g = 1.94$. The value of the effective activation barrier $\Delta_{\rm eff} = |D_{\rm eff}|S^2 = 17.9$ K extracted from the ac data in Ref. [4] ($\Delta_{\rm eff}$, $\tau_0 = 4.89 \times 10^{-9}$ s , parameters of Arrhenius law) fits in the range of published data usually found around 15–23 K (see Refs. [5–7] in Ako *et al.* [34]). This gives an estimate for the effective ZFS constant $D_{\rm eff} = -0.2$ K in the $S = 9$ state. In the temperature domain 1.8–3.5 K ($T > T_b$), the interplay of thermal and quantum relaxation processes of the magnetization occurs. The thermal barrier is therefore "short-cut" by the quantum tunneling of the magnetization, and the obtained $D_{\rm eff}$ value gives the lowest estimate for the theoretical parameter. The upper estimate for $D_{S=9}$ may reach -0.4 K.

IV. MICROSCOPIC MECHANISM OF THE FM EXCHANGE COUPLING

In order to understand why J_1 is much larger than J_2 and J_{bb}, one needs to find all the contributions to these exchange integrals. It is especially nontrivial to explain the difference between J_1 and J_2 because both constants describe coupling between Mn^{3+} and Mn^{2+} ions in a similar geometry.

We will consider the superexchange coming from the virtual hopping of d electrons via p states of ligands, and use the fourth order of the perturbation theory. The perturbation resulting to different energies of $\uparrow\uparrow$ and $\uparrow\downarrow$ states is given by the hopping integral t. The fourth order of the perturbation theory means that we are considering only those paths which consist of four hoppings and the initial and final states are the same. The energy difference between initial and excited states (which appear while electrons hop) define the denominators in Eqs. (3)–(7). The numerators in Eqs. (3)–(7) are given by the corresponding hopping integrals t_{pd} between the ligand p and Mn d orbitals with different coefficients, which take into account the symmetry of the hoppings, number of the hoppings of a given type, etc. The detailed description of this method can be found elsewhere [29,35–37].

One needs to introduce the following parameters to find explicit expressions for the exchange parameters: U is the onsite Coulomb repulsion parameter, and $\Delta_{\rm CT}$ is the charge-transfer energy (energy of the excitation from the ligand $2p$ orbitals to the $3d$ shell of a transition-metal ion). In general, $\Delta_{\rm CT}$ depends both on the valence state of the transition-metal ion and type of the ligand [38,39]. For instance, according to the result of Mizokawa, the charge-transfer energy for Mn^{2+} is $\Delta_{2+} \sim 7$ eV, which is much larger than in the case of the Mn^{3+} ions, for which $\Delta_{3+} \sim 4$ eV [39].

According to the terminology of Ref. [29], there are two important types of the exchange processes related with delocalization and correlation effects. They are sketched in Fig. 6. The delocalization contribution to the exchange interaction involves the transfer of the ligand p electron to one of the Mn ions, while the d electron from another Mn occupies the vacant place in the ligand p shell (after that, both electrons must return to their initial places). The correlation effects are related with the transfer of two p electrons to two d sites on the right and on the left and then back.

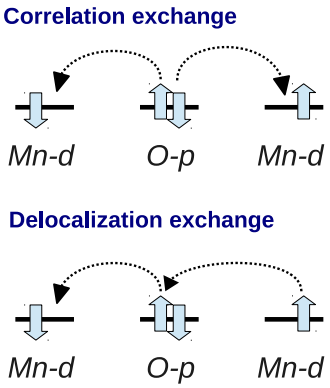

FIG. 6. (Color online) Two types of the contributions to the superexchange according to the notations of Ref. [29].

For simplicity in the analysis, we will neglect the crystal-field splitting between t_{2g} and e_g orbitals (which in general is not small, ∼2 eV, in the case of the transition-metal ions) and the splitting of the Mn^{3+} e_g levels due to the Jahn-Teller effect. These terms will effectively increase the denominators in Eqs. (4)–(7).

A. Delocalization contribution to J_1 and J_2

There are two special features of the studied Mn_4 molecular magnet which must be taken into account to find the expression for the delocalization contribution to the J_1 and J_2 exchange constants.

First of all, the electron transfer from Mn^{3+} to Mn^{2+} (back and forth) is quite different from the transfer from Mn^{2+} to Mn^{3+} (back and forth). Neglecting the intra-atomic Hund's rule coupling (J_H) in the first case, the energies of the excited states (with respect to the energy of the unperturbed state) are Δ_{2+}, $2U$, and again Δ_{2+}. So, this electron transfer is highly unfavorable because it costs $2U$, where $U \sim 4.5$–8 eV [23,40]. In contrast, the second type of the electron transfer (from Mn^{2+} to Mn^{3+} back and forth) costs neither $2U$ nor even U, one only needs to spend the energy V. V is the energy of transfer (excitation) of an electron from Mn^{2+} to Mn^{3+}, determined by the local coordination of these ions and by the intersite Coulomb interaction. Note that this energy V is much smaller than the onsite Coulomb (Hubbard) repulsion U, therefore, the process of the virtual transfer of an electron from Mn^{2+} to Mn^{3+}, leading to superexchange between these ions, costs much less energy than that between the similar Mn ions, Mn^{2+}-Mn^{2+} and Mn^{3+}-Mn^{3+}, and also less than the transfer in the pair Mn^{2+}-Mn^{3+} in the opposite direction, which would correspond to the "reaction" (Mn^{2+},Mn^{3+}) → (Mn^{1+},Mn^{4+}). Correspondingly, this process of virtual hopping from Mn^{2+}

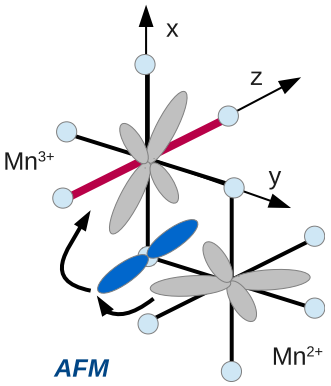

FIG. 7. (Color online) The pair of the t_{2g} orbitals participating in the superexchange interaction between Mn^{3+} and Mn^{2+} in the case of the J_1. There will be the second pair for the same ions, when the orbitals are interchanged and hopping occurs via another common ligand. The ligands are shown as light blue circles, Mn $3d$ orbital in gray, and ligand $2p$ orbitals in blue. Here and in Figs. 8–10, arrows show how the electrons move from one Mn to another.

to Mn^{3+} would give the largest exchange, which agrees with our numerical results.

The intersite Coulomb interaction for Mn was estimated to be ∼0.5 eV using constrained random-phase approximation [41]. The constrained local density approximation (LDA) calculation for charge-ordered Fe_3O_4 (where the number of the d electrons is just slightly larger than in our situation) gives $V = 0.18$ eV [42]. One may expect that $V \ll 2U$ in our case of $Mn_4(hmp)_6$ as well. In effect, the second type of the electron transfer (i.e., from Mn^{2+} to Mn^{3+}) will dominate and one may neglect the first type of the transfer (from Mn^{3+} to Mn^{2+}). This is shown in Figs. 7–10 by arrows.

Moreover, the electron transfer from Mn^{2+} to Mn^{3+} back and forth costs also less charge-transfer energy since one needs to spend Δ_{3+}, and as it was mentioned above $\Delta_{3+} < \Delta_{2+}$. Thus, we see that the charge order strongly modifies the electron-transfer processes (and exchange processes as it will be shown below) and should be explicitly taken into account.

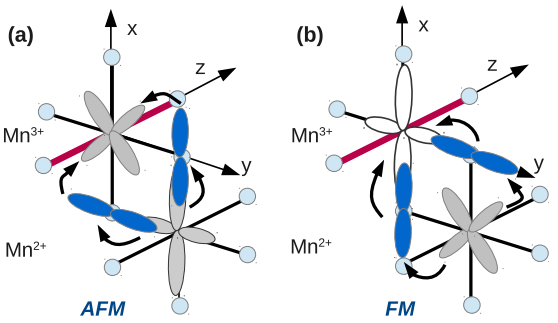

FIG. 8. (Color online) Two t_{2g}/e_g contributions to the superexchange interaction between Mn^{3+} and Mn^{2+} in the case of the J_1. The antiferromagnetic contribution is presented in the left panel (a), while ferromagnetic in the right panel (b). The ligands are shown as light blue circles, half-filled Mn $3d$ orbital in gray, empty x^2-y^2 orbital in white, ligand $2p$ orbitals in blue. The long Mn^{3+}-O is shown in red.

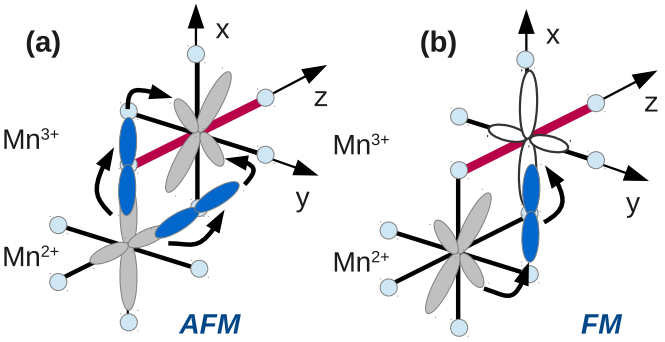

FIG. 9. (Color online) Two t_{2g}/e_g contributions to the superexchange interaction between Mn^{3+} and Mn^{2+} in the case of the J_2. The antiferromagnetic contribution is presented in the left panel (a), while the ferromagnetic in the right panel (b). The ligands are shown as light blue circles, half-filled Mn $3d$ orbital in gray, empty x^2-y^2 orbital in white, ligand $2p$ orbitals in blue. The long Mn^{3+}-O is shown in red.

Second, since the $3d$ shell in the case of the Mn^{2+} is half-filled and in Mn^{3+} is close to half-filling, i.e., to the situation where the energy gain due to the intra-atomic exchange coupling is maximal, one needs to properly count the number of the Hund's rule constants J_H for each electron-transfer process. As we will see in the following, this will additionally stabilize ferromagnetic contributions to the exchange coupling between Mn^{3+} and Mn^{2+}.

We start with the calculation of the contributions coming from exchange coupling between t_{2g} orbitals on Mn^{3+} and Mn^{2+} ions. This term is nearly the same for J_1 and J_2 since all considered orbitals are half-filled on all sites, while the angle dependence of the hoppings can be neglected in the first approximation:

$$J_{1,2}^{t_{2g}/t_{2g}} = \frac{2t_{pd\pi}^4}{\Delta_{3+}^2(V + 4J_H)} \equiv J_0. \tag{3}$$

This contribution is antiferromagnetic and $J_0 > 0$. The factor 2 appears because there are two pairs of the t_{2g} orbitals, which take part in this superexchange process (one of the pairs for J_1 is shown in Fig. 7, while the another one will act via the second common oxygen).

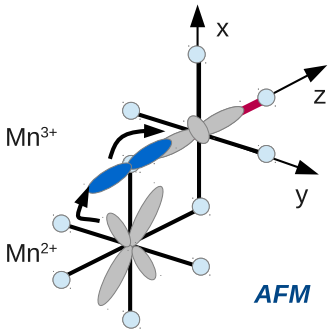

FIG. 10. (Color online) The antiferromagnetic t_{2g}/e_g contributions to the superexchange interaction between Mn^{3+} and Mn^{2+} in the case of the J_2. The ligands are shown as light blue circles, half-filled Mn $3d$ orbital in gray, ligand $2p$ orbitals in blue. The long Mn^{3+}-O is shown in red.

The e_g/e_g contribution in the shared edge geometry is expected to be small since the electrons are supposed to hop via almost orthogonal ligand $2p$ orbitals [23] and will not be considered here. In contrast, the cross terms from the t_{2g} and e_g orbitals are of great importance. They will be different for J_1 and J_2 because the single half-filled e_g orbital of Mn^{3+} is directed differently in the pairs providing J_1 and J_2 exchange couplings.

There are two types of the t_{2g}/e_g contributions. One is the hopping from the half-filled e_g orbital of Mn^{2+} to the half-filled t_{2g} states of Mn^{3+} ($t_{2g} \rightarrow e_g$) and back [see Fig. 8(a)]. These terms are antiferromagnetic and the same for both J_1 and J_2. However, there is also the "opposite" process, hopping of $e_g \rightarrow t_{2g}$, from Mn^{2+} to Mn^{3+} and back. Due to the Jahn-Teller character of the Mn^{3+} ion, with its particular orbital occupation [one e_g electron of Mn^{3+} occupies the $3z^2$-r^2 orbital, where the local z axis is directed along the long Mn-O bonds (see Fig. 1 and red bonds in Figs. 8 and 10)], the contribution of this process would be different for J_1 and J_2. This is explained in detail in the following.

We start with J_1. If the local z axis is directed along the longest Mn^{3+}-O bond, then the x^2-y^2 orbital of Mn^{3+} must be empty, while the $3z^2$-r^2 orbital is half-filled. The expression for the exchange coupling between the half-filled x^2-y^2 orbital of Mn^{2+} and the half-filled xy orbital of Mn^{3+} is very similar to Eq. (3) with the only difference that here one of the t_{pd} hoppings is of the σ symmetry. Since according to Ref. [43] the hopping between the x^2-y^2 and p_x orbitals is $(\sqrt{3}/2)t_{pd\sigma}$ in the given geometry and $t_{pd\sigma} \approx 2t_{pd\pi}$ [30]:

$$J_1^{xy/x^2\text{-}y^2} = \frac{3}{2}\frac{t_{pd\pi}^2 t_{pd\sigma}^2}{\Delta_{3+}^2(V+4J_H)} = 3J_0 \qquad (4)$$

[since exchange occurs via two oxygens, the prefactor equals $2(\sqrt{3}/2)^2 = \frac{3}{2}$]. The orbitals providing this contribution are shown in Fig. 8(a). The exchange coupling given by Eq. (4) is antiferromagnetic.

The ferromagnetic contribution comes from the interaction between the half-filled xy orbital of Mn^{2+} and the empty x^2-y^2 orbital of Mn^{3+}, which are shown in Fig. 8(b). Finding the difference between total energies of ferromagnetic and antiferromagnetic solutions in the perturbation theory, one gets that

$$J_1^{x^2\text{-}y^2/xy} = -\frac{3}{2}\frac{t_{pd\pi}^2 t_{pd\sigma}^2 4J_H}{\Delta_{3+}^2 V(V+4J_H)} = -\frac{12J_0J_H}{V}. \qquad (5)$$

These types of the ferromagnetic terms described by the second Goodenough-Kanamori-Anderson rule [29,36] are usually quite small because instead of the small V there appears U, which is much larger. In effect, these contributions $\sim 1/U^2$ are considerably smaller than the conventional antiferromagnetic superexchange, which is $\sim 1/U$. This is one of the reasons why the insulating transition-metal oxides are mostly antiferromagnets [44]. Moreover, typically the ferromagnets are the systems with the small U ($YTiO_3$ [45], $K_2Cr_8O_{16}$ [46], Ba_2NaOsO_6 [47], etc.). Since, as was mentioned above, in the present system V is less than U this term turns out to be quite efficient. The multiplier $4J_H$, which appears in the numerator in Eq. (5) due to the high-spin state of Mn ions, additionally increases this contribution.

The t_{2g}/e_g contributions to the J_2 can be obtained in a similar manner. The antiferromagnetic coupling between the x^2-y^2 orbital of Mn^{2+} and the t_{2g} orbital is exactly the same as in the case J_1 [the difference is only in the notations: here, the xz orbital is the active one, see Fig. 9(a)] and described by Eq. (4).

The ferromagnetic contribution is also similar, but the coefficients in expression for its value will be different. Due to a different direction of the long Jahn-Teller Mn^{3+}-O bond, only one of the lobes of the empty x^2-y^2 orbital of Mn^{3+} ion will be directed towards Mn^{2+} [see Fig. 9(b)]. As a result, the ferromagnetic term will be just

$$J_2^{x^2\text{-}y^2/xy} = -\frac{3}{4}\frac{t_{pd\pi}^2 t_{pd\sigma}^2 4J_H}{\Delta_{3+}^2 V(V+4J_H)} = -\frac{6J_0J_H}{V}. \qquad (6)$$

In addition to the reduction of the ferromagnetic contribution for this pair (6) as compared to (5), there appears for this bond (due to different direction of the long Mn^{3+}-O bond) also an antiferromagnetic contribution from the hopping between the half-filled xz orbital of Mn^{2+} and the half-filled $3z^2$-r^2 orbital of Mn^{3+}, shown in Fig. 10:

$$J_2^{3z^2\text{-}r^2/xz} = \frac{2t_{pd\pi}^2 t_{pd\sigma}^2}{\Delta_{3+}^2(V+4J_H)} = 4J_0. \qquad (7)$$

Since an opposite hopping from $3z^2$-r^2-Mn^{2+} to xz-Mn^{3+} is also possible, the prefactor 2 appears in the last equation. Thus, one may see that the ferromagnetic t_{2g}/e_g component of J_2 turns out to be suppressed due to a specific orbital order induced by the Jahn-Teller distortions of the $Mn^{3+}O_6$ octahedra, while the antiferromagnetic one is enhanced.

Combining the above-mentioned contributions, one obtains that

$$J_1 = \left(4 - \frac{12J_H}{V}\right)J_0, \qquad (8)$$

$$J_2 = \left(5 - \frac{6J_H}{V}\right)J_0. \qquad (9)$$

Thus, J_1 is ferromagnetic if $V < 3J_H \sim 2.7$ eV. The estimations of V mentioned in Sec. IV A definitely satisfied this condition, so that J_1, as well as J_2, are expected to be ferromagnetic and $|J_1| > |J_2|$. However, care should be taken with V calculated in Refs. [41,42] since in the present consideration V is not only the intersite Coulomb repulsion, but it also includes the effects of the different local environment of the Mn^{3+} and Mn^{2+} ions. In order to calculate V directly, one may use the constraint calculations as proposed in Ref. [42]. This lies beyond the scope of this paper. Here, we only provide the upper limit for the value of V.

One may extract the unscreened value of V, recalculating it as the center of the gravity difference for the $3d$ bands of Mn^{3+} and Mn^{2+} in the LDA approximation. Since there is a different number of the d electrons on these two ions, there will be different contributions from the onsite Coulomb repulsion U to these orbital energies. This correction can be written as $(U - J_H)(n_d - 1/2)$ [22] in the case of Mn ions, where n_d is the number of the d electrons per ion. Taking into account this correction, we obtained the unscreened value of $V \sim 2$ eV, so that even in this situation J_1 must

be ferromagnetic. However, according to Koopmans' theorem, the orbital energies can not be considered as excitation energies (in which we are interested), but are subjected to the orbital relaxation and electron correlation effects, which are the essence of the screening processes and which can be quite efficient [48].

We would like to note that the presented above expressions for the exchange integrals can only be used for the qualitative understanding of the exchange processes in the Mn_4 molecular magnet. The ferromagnetic contributions from the overlap between empty and half-filled orbitals would be reduced by three factors. First of all, one needs to take into account the crystal-field splitting (Δ_{CFS}) between the t_{2g} and e_g shells in an appropriate way, which will modify the denominators in Eqs. (4)–(7) [e.g., in Eq. (4) one will need to substitute $\Delta_{3+} \rightarrow \Delta_{3+} + \Delta_{CFS}$]. Second, as is shown in the Appendix A, there are antiferromagnetic terms related with the correlation contribution to the exchange coupling and these terms are especially important in the case of J_2. Third, there will also be an additional contribution coming from the antiferromagnetic interaction between the half-filled t_{2g} orbitals and the "belt" of the $3z^2$-r^2 orbital (i.e., r^2 part) through the p orbital. Corresponding hopping is not small and equals $t_{pd\sigma}/2$ [43]. This will provide additional contributions to Eqs. (4), (5), and (7) and modify Eqs. (8) and (9), but still leave the qualitative description of the exchange processes correct.

Finally, it is worth mentioning that for the quantitative estimation of different contributions, one needs to know the exact values of the model parameters such as J_H and V.

B. J_{bb} exchange

The same delocalization and correlation effects will be important for the exchange coupling between two Mn^{3+}, i.e., for the J_{bb} exchange constant. However, the sign and the value of the total exchange interaction may strongly depend on the details of the crystal structure: the Mn-O, Mn-Mn distances and the Mn-O-Mn bond angle. The detailed analysis of the J_{bb} does not seem to add much here since first of all it represents the usual superexchange consideration for two Mn^{3+} ions, which can be found elsewhere (e.g., in Ref. [23]), and, second, the value of J_{bb} is quite small.

V. CONCLUSIONS

In this paper, we performed *ab initio* band-structure calculations for the $Mn_4(hmp)_6$ molecular magnet within the density functional theory (DFT) using the GGA + U approximation. The exchange parameters for the Heisenberg model were extracted from the total-energy calculations of several collinear spin configurations. In contrast to a common belief, one of the exchange constants for two pairs of the Mn^{3+} and Mn^{2+} ions (so-called J_{wb}) turns out to be the largest $J_1 = -6.3$ K. Two other exchange couplings are $J_2 = -0.5$ K (another two pairs of Mn^{3+} and Mn^{2+} ions) and $J_{bb} = -0.3$ K (between the Mn^{3+} ions).

The microscopic analysis based on the fourth-order perturbation theory allowed us to establish the mechanism of the strong exchange coupling along the J_1 exchange path. Conventional superexchange between two Mn ions in the edge-sharing geometry is enhanced in $Mn_4(hmp)_6$ by the charge order. The charge disproportionation leads to the situation in which the lowest virtual excitations, contributing to the superexchange, will not be those across the Hubbard gap $\sim U$, but will be those between Mn^{3+} and Mn^{4+}, which cost much smaller energy: the energy V ($\ll U$) stabilizing the charge-ordered state. As a result, the exchange coupling between the empty x^2-y^2 orbital of Mn^{3+} and the half-filled t_{2g} orbitals of Mn^{2+}, according to the second Goodenough-Kanamori-Anderson rule [29], turns out to be quite effective and stabilizes ferromagnetic coupling along the J_1 exchange paths.

In addition to charge order, there is an orbital order in $Mn_4(hmp)_6$, which also has influence on the exchange interaction in this system. The direction of the long Jahn-Teller Mn-O bond in the $Mn^{3+}O_6$ octahedra defines the orientation of the empty x^2-y^2 orbital. This in turn regulates the absolute values of the exchange coupling between different Mn^{3+} and Mn^{2+} pairs making one of them (J_1) larger than the other (J_2).

It is also important that the energy of the first excited state in the exchange process for the ferromagnetic state is reduced by a strong intra-atomic Hund's rule exchange coupling. This is a feature of the Mn^{3+} ion with d^4 electronic configurations that has one empty $3d$ orbital and the energy difference between $(d\uparrow)^5$ and $(d\uparrow)^4(d\downarrow)^1$ states is $4J_H$. For any other configuration (d^3, d^2, etc.), this energy difference between the excited states, according to and against Hund's rule, will be smaller.

The exchange constants calculated in the GGA + U approximation were used for the solution of the quantum Heisenberg model for the given geometry. The magnetic susceptibility obtained by the exact diagonalization method reasonably agrees with the experimentally observed data. This additionally supports the results obtained by the DFT methods. The agreement between theoretical and experimental data may be further improved by "educated" fitting, i.e., fitting, which uses exchange constants obtained in the GGA + U approximation as a starting point. The account of the single-ion anisotropy on the Mn^{3+} sites also makes the agreement better. Although the exchange constants obtained by this fitting are somewhat different from those calculated in the GGA + U ($J_{bb}^{\text{fit},D} = -0.3$ K, $J_1^{\text{fit},D} = -3.6$ K, $J_2^{\text{fit},D} = -0.4$ K, $D^{\text{fit},D} = -0.2$ K), the general tendency is the same: J_1 is the largest exchange coupling.

One of the questions which arises is whether it is possible to increase the values of the ferromagnetic exchanges in the Mn_4 molecular magnets, and what recipes one may provide on the basis of the microscopic model developed in this study. The substitution of all Mn ions by Co, Ni, Cu ions would result in the absence of the empty e_g orbitals, while changing Mn on Ti or V one reduces the energy gain due to the Hund's rule coupling. From this point of view, the pair Cr^{3+} (t_{2g}^3) and Cr^{2+} (Jahn-Teller ion $t_{2g}^3 e_g^1$) could look more promising if one could stabilize Cr^{2+} (which is usually not easy). One may also expect some variations of the exchange constants if the Fe^{4+} and Fe^{3+} instead of the Mn^{3+} and Mn^{2+} ions will be used since the intersite Coulomb repulsion, which

contributes significantly to the energy of the charge-ordered state stabilization, was reported to be quite small for one of the Fe compounds [42]. The substitution of the rare-earth elements instead of the transition-metal ions may lead to a significant gain in the Hund's rule energy, but it will simultaneously decrease the hopping integrals t.

Alternatively, one may try to use not $3d$ but $4d$ or $5d$ elements. These typically have low-spin states with (most of) electrons in the t_{2g} shell and with e_g states often empty and much smaller U (than $3d$ counterparts). Then, one could expect enhancement of ferromagnetic $t_{2g} \rightarrow$ empty e_g contribution. Unfortunately, the crystal-field splitting between t_{2g} and e_g levels for the $4d$ and $5d$ are usually larger, and also the moments of respective ions are smaller than, e.g., those of Mn^{2+}, Mn^{3+} [17,49,50].

Yet another option, which can be proposed, is the substitution of the oxygen by another ligand, e.g., sulfur. The charge-transfer energy Δ_{CT} for the S^{2+} ions is much smaller than for O^{2+} [38] so that it would be chemically possible to substitute some of the oxygens by sulfurs. This may lead to an increase of the exchange coupling.

ACKNOWLEDGMENTS

The authors thank D. Starichenko, who stimulated this study and participated in many interesting discussions about the magnetic properties of the molecular magnets, and A. Katanin and A. Mogilner for providing computational resources and support. This work is supported by the Russian Foundation for Basic Research (Grants No. RFFI-13-02-00374, No. RFFI-13-02-00050, No. RFFI-12-02-31331, No. RFFI 12-02-91371), the Ministry of Education and Science of Russia (Grants No. 12.740.11.0026, No. MK-3443.2013.2, and FCP program), Samsung corporation via the GRO grant, by DFG via 1346 program and Research Grant No. 1484/2-1, by Cologne University via the German excellence initiative, and by Russian Academy of Sciences (Programs No. 12M-23-2054, No. 12-P-2-1017, No. 12-CD-2). The calculations were performed on the "Uran" cluster of the IMM UB RAS.

APPENDIX: CORRELATION CONTRIBUTION TO J_1 AND J_2

Very similar analysis can be performed for the correlation contributions to the J_1 and J_2 exchange parameters. Following, we briefly discuss them and present some of the formulas. Since as was mentioned in Sec. IV A the charge-transfer energy from the O $2p$ to Mn^{2+} $3d$ shell (Δ_{2+}) is much larger than from the O $2p$ to Mn^{3+} $3d$ shell (Δ_{3+}), one may take into account only a part of the correlation contributions related with the charge-transfer energy Δ_{3+}, i.e., the processes, when the first excitation occurs to the $3d$ shell of Mn^{3+}. We will also neglect the terms describing the exchange coupling via orthogonal p orbitals, which are of order or $(t_{pd}^4/\Delta_{3+}^2)[J_H^p/(\Delta_{3+}+\Delta_{2+}+U_{pp})^2]$, where J_H^p is the Hund's rule coupling on the oxygen ion, while U_{pp} is the Coulomb repulsion between two holes in the p shell of oxygen.

The correlation contributions from the half-filled t_{2g} orbitals will be antiferromagnetic and the same for J_1 and J_2:

$$J_{1,2}^{t_{2g}/t_{2g}} \sim \frac{2t_{pd\pi}^4}{\Delta_{3+}^2}\frac{1}{(\Delta_{3+}+\Delta_{2+}+U_{pp})}. \quad \text{(A1)}$$

In the case of J_1, the terms describing the correlation exchange between the empty x^2-y^2 orbital on the Mn^{3+} ion and the half-filled t_{2g} orbitals of the Mn^{2+} and between half-filled t_{2g} orbitals on the Mn^{3+} and the half-filled e_g orbitals of the Mn^{2+} have different signs and nearly cancel each other out.

The direction of the Jahn-Teller distortion of the $Mn^{3+}O_6$ octahedra coincides with one of the Mn^{3+}-O bond forming the Mn^{3+}-Mn^{2+} bond in the case of the J_2 exchange coupling. This upsets the delicate balance between ferromagnetic and antiferromagnetic t_{2g}/e_g terms and makes this contribution antiferromagnetic:

$$J_2^{t_{2g}/e_g} \sim \frac{3}{4}\frac{t_{pd\pi}^2 t_{pd\sigma}^2}{\Delta_{3+}^2}\frac{1}{(\Delta_{3+}+\Delta_{2+}+U_{pp})}. \quad \text{(A2)}$$

This antiferromagnetic term additionally decreases the ferromagnetic contribution to J_2 given in Eq. (6).

[1] R. Sessoli, D. Gatteschi, A. Caneschi, and M. A. Novak, Nature (London) **365**, 141 (1993).
[2] I.-R. Jeon and R. Clérac, Dalton Trans. **41**, 9569 (2012).
[3] D. Gatteschi, R. Sessoli, and J. Villain, *Molecular Nanomagnets* (Oxford University Press, Oxford, 2006).
[4] S.-D. Jiang, S.-S. Liu, L.-N. Zhou, B.-W. Wang, Z.-M. Wang, and S. Gao, Inorg. Chem. **51**, 3079 (2012).
[5] X.-Y. Wang, C. Avendaño, and K. R. Dunbar, Chem. Soc. Rev. **40**, 3213 (2011).
[6] Z. V. Vardeny, *Organic Spintronics* (Taylor & Francis, London, 2010).
[7] R. Winpenny, *Molecular Cluster Magnets*, World Scientific Series in Nanoscience and Nanotechnology (World Scientific, Singapore, 2012).
[8] N. V. Prokofev and P. C. E. Stamp, Phys. Rev. Lett. **80**, 5794 (1998).
[9] A. Michalak, C. M. Canali, M. R. Pederson, M. Paulsson, and V. G. Benza, Phys. Rev. Lett. **104**, 017202 (2010).
[10] F. Rostamzadeh Renani and G. Kirczenow, Phys. Rev. B **85**, 245415 (2012).
[11] D. Boukhvalov, M. Al-Saqer, E. Kurmaev, A. Moewes, V. Galakhov, L. Finkelstein, S. Chiuzbian, M. Neumann, V. Dobrovitski, M. Katsnelson *et al.*, Phys. Rev. B **75**, 014419 (2007).
[12] M. F. Islam, J. F. Nossa, C. M. Canali, and M. Pederson, Phys. Rev. B **82**, 155446 (2010).
[13] D. W. Boukhvalov, L. I. Vergara, V. V. Dobrovitski, M. I. Katsnelson, A. I. Lichtenstein, P. Kögerler, J. L. Musfeldt, and B. N. Harmon, Phys. Rev. B **77**, 180402 (2008).
[14] O. Roubeau and R. Clérac, Euro. J. Inorg. Chem. **2008**, 4325 (2008).
[15] L. A. Kushch, V. D. Sasnovskaya, E. B. Yagubskii, S. S. Khasanov, S. V. Simonov, R. P. Shibaeva, A. V. Korolev, D. V. Starichenko, A. O. Anokhin, V. Y. Irkhin *et al.*, Inorg. Chim. Acta **378**, 169 (2011).
[16] D. I. Khomskii and K. I. Kugel, Phys. Rev. B **67**, 134401 (2003).

[17] S. V. Streltsov and D. I. Khomskii, Phys. Rev. B **86**, 064429 (2012).
[18] V. Barone, A. Bencini, D. Gatteschi, and F. Totti, Chem. Eur. J. **8**, 5019 (2002).
[19] A. Bencini and F. Totti, J. Chem. Theor. Comput. **5**, 144 (2009).
[20] G. Kresse and J. Furthmüller, Phys. Rev. B **54**, 11169 (1996).
[21] J. P. Perdew, K. Burke, and M. Ernzerhof, Phys. Rev. Lett. **77**, 3865 (1996).
[22] V. Anisimov, F. Aryasetiawan, and A. Lichtenstein, J. Phys.: Condens. Matter **9**, 767 (1997).
[23] S. V. Streltsov and D. I. Khomskii, Phys. Rev. B **77**, 064405 (2008).
[24] P. E. Blöchl, O. Jepsen, and O. K. Andersen, Phys. Rev. B **49**, 16223 (1994).
[25] B. Bauer, L. D. Carr, H. G. Evertz, A. Feiguin, J. Freire, S. Fuchs, L. Gamper, J. Gukelberger, E. Gull, S. Guertler *et al.*, J. stat. Mech. (2011) P05001.
[26] S. V. Streltsov, M. A. Korotin, V. I. Anisimov, and D. I. Khomskii, Phys. Rev. B **78**, 054425 (2008).
[27] S. V. Streltsov, M. V. Petrova, V. A. Morozov, G. V. Romanenko, V. I. Anisimov, and N. N. Lukzen, Phys. Rev. B **87**, 024425 (2013).
[28] L. B. Jerzykiewicz, J. Utko, M. Duczmal, P. Starynowicz, and P. Sobota, Eur. J. Inorg. Chem. **2010**, 4492 (2010).
[29] J. B. Goodenough, *Magnetism and the Chemical Bond* (Interscience, New York, 1963).
[30] W. Harrison, *Elementary Electronic Structure* (World Scientific, Singapore, 1999).
[31] S. K. Dey, A. Honecker, P. Mitra, S. K. Mandal, and A. Mukherjee, Eur. J. Inorg. Chem. **2012**, 5814 (2012).
[32] I.-R. Jeon, R. Ababei, L. Lecren, Y.-G. Li, W. Wernsdorfer, O. Roubeau, C. Mathonière, and R. Clérac, Dalton Trans. **39**, 4744 (2010).
[33] L. Lecren, O. Roubeau, C. Coulon, Y.-G. Li, X. F. Le Goff, W. Wernsdorfer, H. Miyasaka, and R. Clérac, J. Am. Chem. Soc. **127**, 17353 (2005).
[34] A. M. Ako, V. Mereacre, I. J. Hewitt, R. Clérac, L. Lecren, C. E. Anson, and A. K. Powell, J. Mater. Chem. **16**, 2579 (2006).
[35] *Correlated Electrons: From Models to Materials*, edited by E. Pavarini, E. Koch, F. Anders, and M. Jarrell (Forschungszentrum Jülich GmbH, Jülich, Germany, 2012).
[36] D. I. Khomskii, *Basic Aspects of the Quantum Theory of Solids: Order and Elementary Excitations* (Cambridge University Press, New York, 2010).
[37] M. Ziese and M. J. Thornton, *Spin Electronics*, Lecture Notes in Physics (Springer, Berlin, 2001).
[38] A. E. Bocquet, T. Mizokawa, T. Saitoh, H. Namatame, and A. Fujimori, Phys. Rev. B **46**, 3771 (1992).
[39] A. Ushakov, S. V. Streltsov, and D. I. Khomskii, J. Phys.: Condens. Matter **23**, 445601 (2011).
[40] J. E. Medvedeva, M. A. Korotin, V. I. Anisimov, and A. J. Freeman, Phys. Rev. B **65**, 172413 (2002).
[41] T. Miyake and F. Aryasetiawan, Phys. Rev. B **77**, 085122 (2008).
[42] V. I. Anisimov, I. S. Elfimov, N. Hamada, and K. Terakura, Phys. Rev. B **54**, 4387 (1996).
[43] J. C. Slater and G. F. Koster, Phys. Rev. **94**, 1498 (1954).
[44] D. Khomskii, Lith. J. Phys. **37**, 65 (1997).
[45] S. V. Streltsov, A. S. Mylnikova, A. O. Shorikov, Z. V. Pchelkina, D. I. Khomskii, and V. I. Anisimov, Phys. Rev. B **71**, 245114 (2005).
[46] T. Toriyama, A. Nakao, Y. Yamaki, H. Nakao, Y. Murakami, K. Hasegawa, M. Isobe, Y. Ueda, A. Ushakov, D. Khomskii *et al.*, Phys. Rev. Lett. **107**, 266402 (2011).
[47] A. S. Erickson, S. Misra, G. J. Miller, R. R. Gupta, Z. Schlesinger, W. A. Harrison, J. M. Kim, and I. R. Fisher, Phys. Rev. Lett. **99**, 016404 (2007).
[48] I. V. Solovyev and M. Imada, Phys. Rev. B **71**, 045103 (2005).
[49] S. V. Streltsov, Phys. Rev. B **88**, 024429 (2013).
[50] H. D. Zhou, A. Kiswandhi, Y. Barlas, J. S. Brooks, T. Siegrist, G. Li, L. Balicas, J. G. Cheng, and F. Rivadulla, Phys. Rev. B **85**, 041201 (2012).